Max-Planck-Institut
für Mathematik
in den Naturwissenschaften
Leipzig

Monte Carlo simulations of
two-dimensional charged bosons

by

Stefania De Palo, Sergio Conti, and Saverio Moroni

Monte Carlo simulations of two-dimensional charged bosons

S. De Palo,[1] S. Conti,[2] and S. Moroni[3]

[1] *Dipartimento di Fisica, Università di Roma "La Sapienza",*

P.le Aldo Moro 5, 00185 Rome, Italy

[2] *Max Planck Institute for Mathematics in the Sciences,*

Inselstrasse 22, 04103 Leipzig, Germany

[3] *SMC INFM, Dipartimento di Fisica,*

Università di Roma "La Sapienza",

P.le Aldo Moro 5, 00185 Rome, Italy

(Dated: June 11, 2003)

Abstract

Quantum Monte Carlo methods are used to calculate various ground state properties of charged bosons in two dimensions, throughout the whole density range where the fluid phase is stable. Wigner crystallization is predicted at $r_s \simeq 60$. Results for the ground state energy and the momentum distribution are summarized in analytic interpolation formulas embodying known asymptotic behaviors. Near freezing, the condensate fraction is less than 1%. The static structure factor $S(k)$ and susceptibility $\chi(k)$ are obtained from the density-density correlation function in imaginary time, $F(\mathbf{k}, \tau)$. An estimate of the energy of elementary excitations, given in terms of an upper bound involving $S(k)$ and $\chi(k)$, is compared with the result obtained via analytic continuation from $F(\mathbf{k}, \tau)$.

PACS numbers: 02.70.Ss, 05.30.Jp

I. INTRODUCTION

The two-dimensional fluid of point-like spinless bosons interacting with a $1/r$ potential has drawn attention in the literature[1] as a model in quantum statistical mechanics which parallels the physically more relevant fluid of electrons. At zero temperature, the model is specified by the coupling parameter $r_s = 1/\sqrt{\pi n} a_B$, where n is the density and a_B the Bohr radius. For small r_s the system is a weakly coupled fluid, well described by the Random Phase Approximation,[2] whereas it becomes strongly correlated and eventually undergoes Wigner crystallization upon increasing r_s. Several results for the ground state energy, static structure, screening properties and elementary excitations have been reported using the Correlated Basis Function theory,[1,3] various implementation of the Singwi-Tosi-Land-Sjölander (STLS) formalism,[4,5] and the Overhauser model.[6] The momentum distribution has been calculated for low r_s in the Bogolubov approximation.[7] A comparison between the STLS results for the $1/r$ potential and the $\ln(r)$ potential has been reported by Moudgil *et al.*[8]

Although the charged boson model may find applications to superconductors, either as a system of bound electron pairs[9] or in terms of an effective action with Fermionic degrees of freedom integrated out,[10] no direct realization of the system is experimentally available. Therefore numerical results provided by quantum Monte Carlo (QMC) simulations constitute the only reliable benchmark for analytic approaches. Extensive simulation results are available for 3D charged bosons[11,12] and for the 2D system with the $\ln(r)$ interaction.[13–15]

In this work we present QMC results for several ground state properties of the 2D fluid of charged bosons with the $1/r$ potential. We use two different algorithms, namely diffusion Monte Carlo (DMC),[16] which is more efficient in the calculation of mixed averages, and reptation quantum Monte Carlo (RQMC),[17] which gives easier access to correlations in imaginary time. The exact ground state energy and the mixed estimate[16] of the one-body density matrix are calculated with the former. Unbiased estimates of the static structure factor and the susceptibility are instead obtained, using RQMC, from the auto-correlation in imaginary time of the density fluctuation operator. The inverse Laplace transform of the same auto-correlation function yields valuable information on the spectrum of elementary excitations.

II. METHOD

Quantum Monte Carlo is the method of choice for strongly interacting bosonic systems in their ground state, because it yields exact numerical results for a number of quantities, subject only to known statistical errors.

The DMC method[16] samples a probability distribution proportional to the "mixed distribution" $f(R) = \Phi(R)\Psi(R)$, where $R = \{\mathbf{r}_1, \cdots, \mathbf{r}_N\}$ is a point in the $2N$-dimensional configuration space of the system, $\Psi(R)$ is a trial wave-function, and $\Phi(R)$ is the ground-state wave-function. The exact ground state energy is obtained as the average over the mixed distribution of the local energy, $E_L(R) = \Psi(R)^{-1}H\Psi(R)$. For a general operator not commuting with the Hamiltonian, ground-state averages can be approximated by the extrapolated estimate (twice the average over the mixed distribution minus the variational estimate),[16] which leads to an error quadratic in the difference $(\Phi - \Psi)$. Our results for the one-body density matrix are given in terms of this extrapolated estimate, as in Ref. 12.

For operators diagonal in R we avoid mixed estimates resorting to the RQMC method[17] (one could alternatively use the forward walking technique[18] within the DMC method). In RQMC, the evolution in imaginary time of the system is represented by a time-discretized path $X = \{R_0, \cdots, R_M\}$. The algorithm samples the distribution $P(X) = \Psi(R_0)^2 \Pi_{i=1}^{M} G(R_{i-1} \to R_i; \epsilon)$, where $G(R \to R'; \epsilon)$ is a short-time approximation to the importance-sampled Green's function $\Psi(R')\langle R'| \exp(-\epsilon H)|R\rangle\Psi(R)^{-1}$. Assuming M is large enough, the inner time slices of the path are individually sampled from the distribution $\Phi(R)^2$, and sequentially sampled according to the quantum dynamical fluctuations in the ground state. Pure estimators, $\langle\Phi|O|\Phi\rangle = \langle\langle O(R_i)\rangle\rangle$, and imaginary-time correlation functions, $c(\tau) = \langle\langle O(R_i)O(R_{i+n})\rangle\rangle$, are thus readily accessible (here $\langle\langle\cdot\rangle\rangle$ means average over the random walk in the space of quantum paths X, and $\tau = n\epsilon$).[17]

In all simulations we consider a system of N particles in a square cell with periodic boundary conditions. The trial function is chosen of the pair product form, $\Psi(R) = \exp(-\sum_{ij} u(|\mathbf{r}_i - \mathbf{r}_j|))$, where $u(r)$ is the RPA pseudopotential following Ref. 19. Both the pseudopotential and the Coulomb interaction are evaluated using generalized Ewald sums.[19] As usual,[11,19] we estimate the finite-size effect on the ground-state energy from variational Monte Carlo simulations. Variational energies E_N, calculated with N in the range 25–200, are used to determine the best–fit parameter in the form $E_\infty = E_N + a(r_s)/N + b(r_s)/N^2$.

Assuming that the same size dependence holds for the exact DMC energies, the optimal parameters $a(r_s)$ and $b(r_s)$ are then used to extrapolate to the thermodynamic limit the result of a single DMC simulation with $N = 52$. Other quantities have comparatively smaller finite-size errors, typically below the statistical accuracy of the present simulations.

III. RESULTS

A. Ground-state energy

The DMC ground state energies of the 2D bosonic fluid in the thermodynamic limit are compared in Table I with the results obtained with the Singwi–Tosi–Land–Sjölander (STLS) method by Gold,[5] with a parametrized wave function approach by Sim, Tao and Wu[3] and within the Hypernetted Chain Approximation (HNC) by Apaja et al..[1] While all computations agree qualitatively, we note that the agreement between HCN and the exact DMC results is particularly good. Our DMC results can be accurately reproduced by the parametrized function:

$$E_g(r_s) = -[a_0 r_s^{b_0} + a_1 r_s^{b_1} + a_2 r_s^{b_2} + a_3 r_s^{b_3}]^{-c} \tag{1}$$

where a_0 and b_0 are fixed by the small r_s behavior[1] ($E(r_s \to 0) \simeq -1.29355/r_s^{2/3}$), b_1 is fixed requiring a constant sub-leading term for $r_s \to 0$, b_2 and b_3 by requiring leading terms in r_s^{-1} and $r_s^{-3/2}$ for $r_s \to \infty$. The final values of the parameters are $c = 7/40$, $a_0 = 0.2297$, $a_1 = 0.161$, $a_2 = 0.0594$, $a_3 = 0.01017$, $b_0 = 80/21$, $b_1 = 94/21$, $b_2 = 73/14$ and $b_3 = 40/7$. The reduced χ^2 for the fit with 4 parameters and 7 data points is 1.5 at $r_s = 1$. The above interpolation formula allows to obtain, by means of the virial theorem, the unbiased estimator of the average kinetic energy $\langle ke \rangle = -d(r_s E_g)/dr_s$ as well as of the inverse compressibility $1/\rho K_T = -\frac{r_s}{4}[\frac{\partial E_g}{\partial r_s} - r_s \frac{\partial^2 E_g}{\partial r_s^2}]$, both reported in Table I.

In Fig. (1) our results are compared with the previous DMC results by Rapisarda and Senatore[20] for 2D fermions and for the 2D Wigner crystal. In two dimensions bosons crystallize at $r_s \simeq 60$ and fermions at $r_s \simeq 34$. The difference in critical density is analogous to the difference obtained in the 3D case, where bosons crystallize at $r_s = 160$ and fermions at $r_s = 100$.[11]
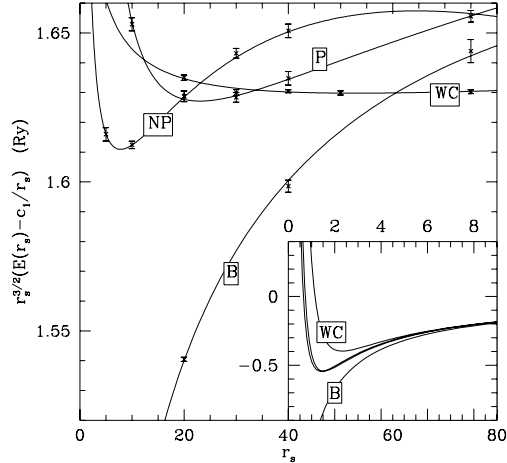
FIG. 1: Ground-state energy for 2D triangular Wigner crystal (WC), bosons (B), unpolarized (UP) and polarized (P) fermions as a function of r_s. Wigner crystal and fermion data are from Ref. 20. On purpose of clarity we plotted $r_s^{3/2}(E(r_s) - c_1/r_s)$, with $c_1 = -2.2122$, while the inset shows the corresponding $E(r_s)$ curves. Points with error bars are size-extrapolated DMC results, continuous curves are analytical fits.

TABLE I: Ground state energy for bosons from VMC and DMC, extrapolated to the bulk limit and compared with estimates from approximate theories. We also give the average kinetic energy and inverse compressibility obtained from Eq. (1). All values are in Rydberg per particle, the digits in parenthesis represent the error bar in the last digit.

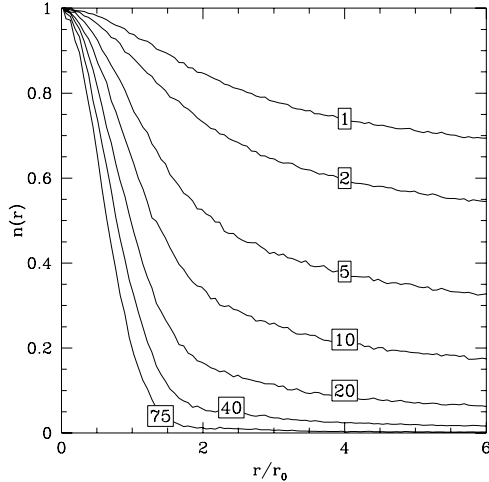| r_s	$E^{(DMC)}$	$E^{(VMC)}$	HNC[1]	STW[3]	STLS[5]	$\langle ke \rangle$	$1/nK_T$
1	-1.1448(5)	-1.14269(7)	-1.1458	-1.1062	-	0.2903	-0.531
2	-0.6740(2)	-0.67192(6)	-0.6740	-0.6631	-0.6484	0.1442	-0.3582
5	-0.31903(5)	-0.317456(6)	-0.3185	-0.3133	-0.3078	0.04896	-0.187
10	-0.17480(5)	-0.17385(3)	-0.1741	-0.16685	-0.1724	0.01961	-0.1097
20	-0.093387(8)	-0.092903(3)	-0.0928	-0.086024	-0.0959	0.007533	-0.06177
40	-0.048986(8)	-0.048737(2)	–	–	–	0.00286	-0.03359
75	-0.026965(6)	-0.0268246(8)	–	–	–	0.001189	-0.01892

5

FIG. 2: One–body density matrix $n(r)$ at $r_s =$1, 2, 5, 10, 20, 40 and 75

B. Momentum distribution

The one–body density matrix $n(r)$ and its Fourier transform, the momentum distribution $n(k)$, have been computed performing random displacements of particles on the sampled configurations as explained in Ref. 13.

At variance with the 3D case,[12] the standard procedure leads to strong size effects due to the slow convergence of $n(r)$ to its asymptotic limit $n_0 = \lim_{r\to\infty} n(r)$. We removed the size-effect adopting the correction proposed by Magro and Ceperley[13] for 2D bosons with $\ln r$ interactions. Our results for the one–body density matrix are shown in Fig. (2).

Extending to the 2D case the discussion presented for 3D charged bosons in Ref. 21, we fix the divergence of the momentum distribution at small k

$$n(k \to 0) \simeq \frac{n_0}{4S(k)} \simeq \frac{n_0 \sqrt{r_s/2}}{(kr_0)^{3/2}} \tag{2}$$

where n_0 is condensate fraction, and $r_0 = r_s a_B$. The cusp condition[22] instead gives information on the short–range behavior of the momentum distribution:

$$n(k \to \infty) \simeq \frac{4r_s^2 g(0)}{(kr_0)^6} \tag{3}$$

where $g(0)$ is the pair correlation function at $r = 0$. Moreover, at small density, we expect the momentum distribution to be approximately Gaussian, in agreement with harmonic theory for the crystalline phase.

6

TABLE II: Best fit parameters for equation (4). The last line reports the value of $g(0)$ from Fig. (4) as used in the fit of $n(k)$.

r_s	1	2	5	10	20	40	75
n_0	0.531	0.38	0.176	0.0677	0.018	0.001	0.0007
a_0	0.839	0.853	0.475	0.977	0.861	1.21	2.59
a_1	44	3.5	5.46	–	–	–	–
a_2	-0.086	0.492	2.17	1.96	1.05	0.946	0.098
a_3	0.696	0.56	-2.1	-1.13	-0.08	-0.74	0.627
a_4	1.13	0.226	0.23	-0.01	-0.163	0.184	-0.103
a_5	0.135	0.192	0.28	0.7	-0.006	-0.014	-0.024
a_6	-111	-6.07	1.12	-1.52	0.849	3.44	0.576
a_7	6.98	2.29	1.45	1.86	2.61	1.99	2.59
g_0	0.21	0.078	0.01	-	-	-	-
$n_0{}^7$	0.537	0.398	0.230	-	-	-	-

We have collected all this information in a fitting formula to interpolate the DMC data for the momentum distribution $n(k)$:

$$n(k) = (2\pi)^2 \rho n_0 \delta^2(k) + \frac{n_0 \sqrt{r_s/2}}{\kappa^{3/2}} e^{-\kappa^2/a_0^2} + \frac{4g(0)r_s^2}{a_1^6 + \kappa^6}$$
$$+ \left(\frac{a_2}{\sqrt{\kappa}} + a_3 + a_4\sqrt{\kappa} + a_5\kappa \right) e^{-(\kappa^2 - \kappa a_6)/a_7^2}$$

where $\kappa = kr_0$. Given the known values of the density and of $g(0)$ (see next section), we determined the remaining parameters by a least–squares fit to the DMC data on $n(k)$, $n(r)$ and on the average kinetic energy.

Table II contains the best–fit parameters and the resulting value of the condensate fraction n_0. The condensate fraction decreases very rapidly with increasing r_s, the depletion being already 50% at $r_s = 1$, in agreement with the result of the Bogolubov theory[7] (in 3D[12] a similar depletion occurs at $r_s = 5$). For large couplings, the Bogolubov theory overestimates the condensate fraction. In a wide density range in the liquid phase, say $r_s > 20$, n_0 is of

7

the order of 1% or less. Such small values, obtained by fitting Eq. 4 to the extrapolated estimates from the simulation, are presumably meaningful only as an indication of the order of magnitude.

C. Imaginary-time correlation functions: static response function and static structure factor

Information on charge response properties of the system like screening, plasma oscillations or polarization are contained in the imaginary time density-density correlation function:

$$F(k,\tau) = \frac{1}{N}\langle \rho_{\mathbf{k}}(\tau)\rho_{\mathbf{k}}(0)\rangle = \frac{1}{2\pi}\int_{-\infty}^{\infty} e^{-\tau\omega} S(k,\omega), \tag{4}$$

where $\rho_{\mathbf{k}}(\tau) = \sum_i e^{i(\mathbf{k}\cdot\mathbf{r})}$ and $S(k,\omega)$ is the dynamical response function. The correlation functions $F(k,\tau)$ have been computed with RQMC for systems of 56 particles.

The static structure factor $S(k)$ is readily obtained from the imaginary-time density-density correlation function as:

$$S(k) = \int_0^{\infty} d\omega\ S(k,\omega) = F(k,0). \tag{5}$$

In Fig. (3) we report the behavior of $S(k)$ for various densities. As r_s increases and approaches the crystallization density, a sharp peak develops in correspondence with the first lattice wave-vector of the 2D Wigner crystal, $kr_0 = (2\pi\sqrt{3})^{1/2} \simeq 3.3$.

In Fig. (4) we report the pair distribution function:

$$g(r) = \frac{1}{N\rho}\sum_{i\neq j}\langle\delta(|\mathbf{r}_i - \mathbf{r}_j| - r)\rangle. \tag{6}$$

At low density $g(r)$ develops a high peak and long-range oscillations typical of a system approaching localization. As the density increases the effective repulsion between particles decreases and overlapping between charges becomes possible. The behavior of $S(k)$ and $g(r)$ is qualitatively in agreement with the findings of Apaja et al.,[1] but for both functions the Monte Carlo results show more pronounced effects of correlations at low densities.

The static response function $\chi(k)$ can be evaluated from the relation

$$\chi(k) = -2\int_0^{\infty}\frac{S(k,\omega)}{\omega}d\omega = -2\int_0^{\infty} F(k,\tau)d\tau. \tag{7}$$
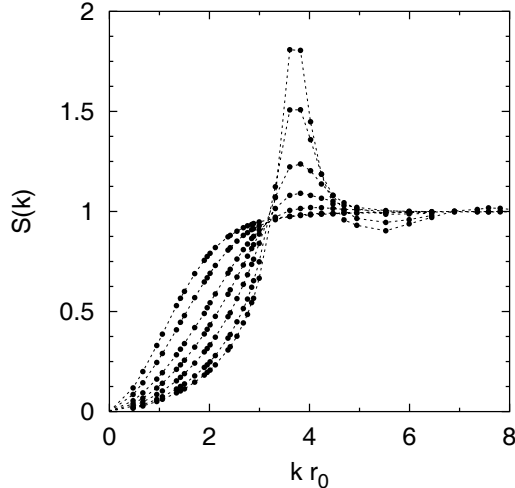
FIG. 3: Static structure factor $S(k)$ as a function of kr_0 for $r_s = 1, 2, 5, 10, 20, 40, 60$. Lines are only guide to the eyes.
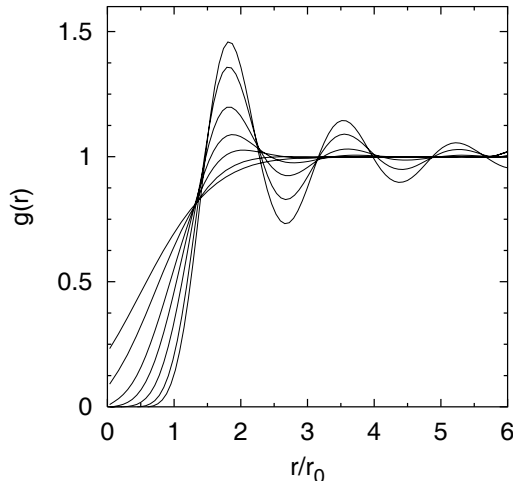

FIG. 4: The pair-distribution function for $r_s = 1, 2, 5, 10, 20, 40$ and 60 (cubic spline interpolation of Monte Carlo data). Higher peaks correspond to higher values of r_s.

In Fig. (5) we report the static effective interaction $v_k/\epsilon(k,0)$ where v_k is the Coulomb interaction and $\epsilon(k,0) = 1/[1 + v_k \chi(k,0)]$ is the static dielectric function. At low k the effective interaction is given the compressibility sum rule,

$$\lim_{k \to 0} \frac{v_k}{\epsilon(k,0)} = \frac{1}{\rho K_T}, \tag{8}$$

while in the short-wavelength limit it behaves like the Coulomb interaction. The minimum of $v_k/\epsilon(k,0)$ deepens and shifts to larger k upon increasing r_s. We note that a negative dielectric function cannot be interpreted as a signal of instability of the bosonic fluid due to
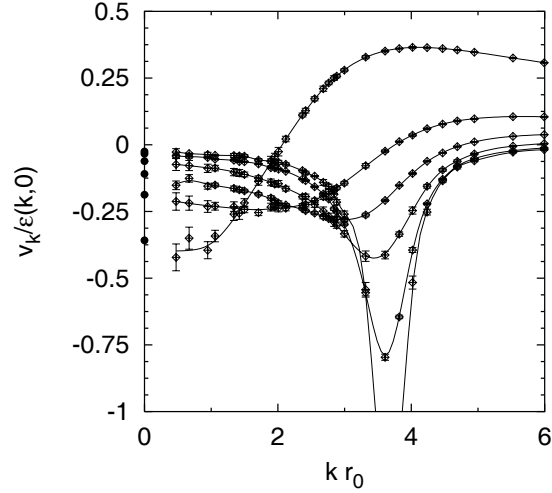
9

FIG. 5: Effective interaction for $r_s = 2, 5, 10, 20, 40$ and 60 (open symbols, Monte Carlo data; lines, cubic spline interpolations). Deeper minima correspond to lower densities. The solid dots at $k = 0$ are the values of $1/\rho K_T$ from Tab. I.
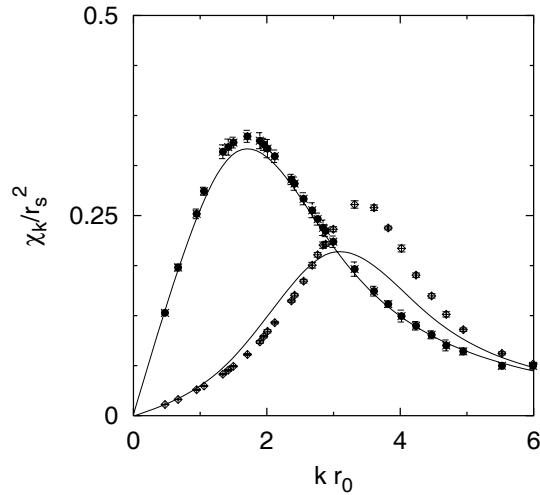

FIG. 6: The static response function $\chi(k)$ at $r_s = 1$ (solid dots) and $r_s = 10$ (open diamonds). The solid lines are from Apaja et al..[1]

the presence of the rigid background. As in the case of the structural properties, in the large coupling regime the Monte Carlo data for the effective potential show more pronounced features than the results of Apaya et al..[1] This is shown, in terms of the static response function $\chi(k)$, in Fig. (6).
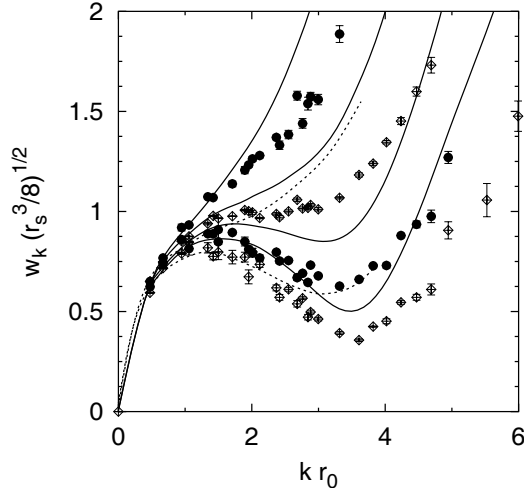
10

FIG. 7: The excitation spectra for $r_s = 2, 5, 10, 20$ (full circles and open diamonds) are compared with their respective upper-bound ω_k^{min} (solid lines). Dashed curves corresponds to data from Ref. 1 for $r_s = 5$ and $r_s = 20$. Curves with deeper minimum corresponds to lower densities.

D. Excitation spectrum

The elementary excitations spectrum of the density fluctuation is contained in the dynamic structure factor:

$$S(k, \omega) = \sum_n |\langle n|\rho_k|0\rangle|^2 \delta(\omega - \omega_{n0}). \tag{9}$$

We estimate the energy dispersion of the collective excitation by fitting the imaginary time dependence of $F(k, \tau)$ with $F(k, \tau) = A(k)e^{-\omega_1(k)\tau} + B(k)e^{-\omega_2(k)\tau}$. This amounts to represent the dynamical structure factor $S(k, \omega)$ as the sum of two delta functions. When a single mode has a dominating spectral weight, its dispersion $\omega_1(k)$, is reproduced reasonably well,[17] regardless of the representation chosen for the remaining part of the spectrum (a delta function at $\omega_2(k)$ in this case).

Moreover, combining our results for $\chi(k)$ and $S(k)$ we obtain, by means of a sum-rules approach,[12,23] a rigorous upper bound for the plasmon dispersion:

$$\omega_k^{min} \leq \frac{2\rho S(k)}{\chi(k)}. \tag{10}$$

At low k a single mode exhausts the sum rule. In this case, the upper bound in Eq. (10) becomes an equality and the strength of the excitation coincides with $S(k)$.

In Fig. 7 we show our results for the excitation energies extracted directly from $F(k, \tau)$ and compare them with their corresponding upper-bounds, at different densities. On increasing
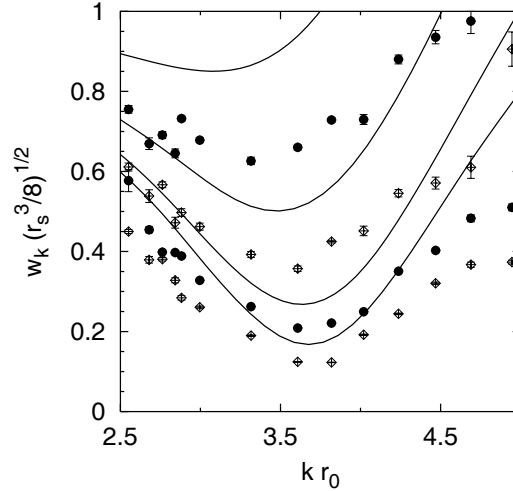
11

FIG. 8: Excitation spectrum near the rotonlike minimum for $r_s = 10, 20, 40, 60$. Full circles and open diamonds, data from two-exponentials fit to $F(k, \tau)$; solid lines, upper-bounds from Eq. 10.

r_s a roton–like mode, close to the first reciprocal lattice vector of the Wigner crystal, develops and softens. The evolution of this minimum as the crystallization transition is approached is shown in more detail in Fig. (8).

In conclusions, we have presented an extensive QMC study of ground-state properties of 2D charged bosons. The present results constitute a valuable benchmark for theoretical approaches, showing their range of validity.

[1] V. Apaja, J. Halinen, V. Halonen, E. Krotscheck, and M. Saarela, Phys. Rev. B **55**, 12925 (1997).

[2] D. F. Hines and N. E. Frankel, Phys. Rev. B **20**, 972 (1979).

[3] H.-K. Sim, R. Tao and F. Y. Wu, Phys. Rev. B **34**, 7123 (1986).

[4] C. I. Um, W. H. Kahng, E. S. Yim, and T. F. George, Phys. Rev. B **41**, 259 (1990).

[5] A. Gold, Z. Phys. B **89**, 1 (1992).

[6] B. Davoudi, M. Polini, R. Asgari, M. P. Tosi, cond-mat/0210664.

[7] E. Strepparola, A. Minguzzi, and M. P. Tosi, Phys. Rev. B **63**, 104509 (2001).

[8] R. K. Moudgil, P. K. Ahluwalia, K. Tankeshwar, K. N. Pathak, Phys. Rev. B **55** , 544 (1997).

[9] A. S. Alexandrov and N. F. Mott, Supercond. Sci. Technol. **6**, 215 (1993); A. S. Alexandrov and P. P. Edwards, Physica C **331**, 97 (2000).

[10] S. De Palo, C. Castellani, C. Di Castro, and B. K. Chakravarty, Phys. Rev. B **60** , 564 (1999).

[11] D. M. Ceperley and B. J. Alder, Phys. Rev. Lett. **45**, 566 (1980); D. M. Ceperley and B. J. Alder, J. Phys. Colloq. 7, C295 (1980).

[12] S. Moroni, S. Conti, and M. P. Tosi, Phys. Rev. B **53**, 9688 (1996).

[13] W. R. Magro and D. M. Ceperley, Phys. Rev. Lett. **73**, 826 (1994).

[14] W. R. Magro and D. M. Ceperley, Phys. Rev. B **48**, 411 (1993).

[15] Henrik Nordborg and Gianni Blatter, Phys. Rev. Lett. **79**, 1925 (1997).

[16] W. M. C. Foulkes, L. Mitas, R. J. Needs, and G. Rajagopal, Rev. Mod. Phys. **73**, 33 (2001).

[17] S. Baroni and S. Moroni, Phys. Rev. Lett. **82**, 4745 (1999).

[18] K. S. Liu, M. H. Kalos and G. V. Chester, Phys. Rev. A **10**, 303 (1974).

[19] D. M. Ceperley, Phys. Rev. B **18**, 3126 (1978).

[20] F. Rapisarda and G. Senatore, Aust. J. Phys. **49**, 161 (1996).

[21] M. L. Chiofalo, S. Conti and M.P. Tosi, J. Phys.: Condens. Matter **8**, 1921 (1996).

[22] A. K. Rajagopal and J. C. Kimball, Phys. Rev. B **15**, 2819 (1977).

[23] S. Stringari, Phys. Rev. B **46**, 2974 (1992); J. Boronat, J. Casulleras, F. Dalfovo and S. Stringari, S. Moroni, Phys. Rev. B **52**, 1236 (1995).